

Efficient Tensor Contraction via Fast Count Sketch

Xingyu Cao^{a,*}, Jiani Liu^a

^a*School of Information and Communication Engineering, University of Electronic Science and Technology of China (UESTC), Chengdu, 611731, China.*

Abstract

Sketching uses randomized Hash functions for dimensionality reduction and acceleration. The existing sketching methods, such as count sketch (CS), tensor sketch (TS), and higher-order count sketch (HCS), either suffer from low accuracy or slow speed in some tensor based applications. In this paper, the proposed fast count sketch (FCS) applies multiple shorter Hash functions based CS to the vector form of the input tensor, which is more accurate than TS since the spatial information of the input tensor can be preserved more sufficiently. When the input tensor admits CANDECOMP/PARAFAC decomposition (CPD), FCS can accelerate CS and HCS by using fast Fourier transform, which exhibits a computational complexity asymptotically identical to TS for low-order tensors. The effectiveness of FCS is validated by CPD, tensor regression network compression, and Kronecker product compression. Experimental results show its superior performance in terms of approximation accuracy and computational efficiency.

Keywords: accelerated tensor contraction, random projection,

*Corresponding author.

Email addresses: xingyucao@std.uestc.edu.cn (Xingyu Cao),
jianiliu@std.uestc.edu.cn (Jiani Liu)

dimensionality reduction, tensor decomposition, deep neural network
compression

1. Introduction

Many real-world data exhibit multi-dimensional form and can be naturally represented by tensors. Tensor decomposition is an essential tool for multi-way data analysis [1, 2, 3, 4]. As a generalization of the matrix product, tensor contraction is widely used in tensor factorization based methods [5, 6, 7, 8]. However, tensor contraction is time-consuming and costs a lot of memory, especially when the data size is large. To this end, some randomization methods are developed to accelerate tensor decomposition algorithms [9, 10, 11, 12, 13].

Sketching adopts this randomization strategy, which succinctly maps the input data into a low-dimensional sketched space while preserving certain data properties. Unlike general random sampling, the sketching techniques commonly use random sparse matrices with certain structure, which are more efficient for computation with guaranteed performance [14, 15]. Sketching methods are successfully applied in low-rank approximation [15, 16, 17], regression [14, 15, 18], etc.

Charikar et al. [19] propose a simple and effective sketching method termed Count sketch (CS) to estimate the frequency of items in a data stream. They use a random Hash function pair to map the input vector into a low-dimensional sketched space. Pagh [20] combines CS of the outer product of two vectors with fast Fourier transform (FFT) to accelerate matrix multiplication compression. Despite the effectiveness of CS, it only applies

to vector-valued data. When the input data is a high-order tensor, it needs to vectorize the tensor and generate a long pair of Hash functions to match the dimension of the vectorized tensor. Therefore, the storage cost for the Hash functions is high.

Pham et al. [21] propose tensor sketch (TS) by extending CS to high-dimensional space for polynomial kernel approximation. TS is widely used in multi-dimensional data processing tasks such as tensor decomposition [7, 22, 23, 24], Kronecker product regression [25, 26], and neural network compression [27, 28].

Although TS is suitable for tensor data, it inadequately exploits the multi-dimensional structure information of the input tensor by directly sketching it into a vector. To fully exploit the multi-dimensional structure information within tensors, Shi et al. [29] propose higher-order count sketch (HCS), which sketches the input tensor into a lower-dimensional one of the same order. However, HCS suffers from low accuracy and slow speed in some tensor based applications. Therefore, it is essential to develop a new sketching method that can achieve good approximation quality with competitive running speed.

In this paper, we propose a fast count sketch (FCS) which combines the advantages of these three sketching methods. For a general tensor \mathcal{T} , FCS applies multiple short Hash functions based CS on $\text{vec}(\mathcal{T})$ instead of generating a long Hash function pair directly as done by $\text{CS}(\text{vec}(\mathcal{T}))$. In this way, FCS costs less storage for Hash functions, since only the short ones are stored. The computational complexity of FCS for general tensors is $O(\text{nnz}(\mathcal{T}))$, where $\text{nnz}(\cdot)$ represents the number of non-zero elements. Meanwhile, compared with TS, the integrated Hash functions allow FCS to exploit the spatial in-

formation within tensors more sufficiently, which results in more accurate estimation, especially when the Hash length of Hash functions is short. Specially, suppose a tensor \mathcal{T} admits CANDECOMP/PARAFAC decomposition (CPD) [30, 31], FCS can be accelerated by FFT, which exhibits a computational complexity asymptotically identical to TS for low-order tensors, and is much faster than HCS.

To verify the effectiveness of FCS, we apply it to two CPD algorithms named robust tensor power method (RTPM) [5] and alternating least squares (ALS) [32], which involve two specific tensor contractions $\mathcal{T}(\mathbf{u}, \mathbf{u}, \mathbf{u})$ and $\mathcal{T}(\mathbf{I}, \mathbf{u}, \mathbf{u})$. Theoretical proofs guarantee that the estimation by FCS is more accurate than TS when the same Hash functions are used. Experiments on both synthetic and real-world datasets demonstrate FCS achieves better approximation performance with competitive running speed, compared to various counterparts. We also apply FCS to compress the weight tensor of a tensor regression network (TRN) [33] tailed with a CP layer. Experimental results demonstrate FCS achieves better classification performance than other counterparts under various compression ratios. Finally, we compress the Kronecker product and tensor contraction using FCS. Experimental results show that compared to CS, FCS takes less compressing time and Hash memory; compared to HCS, FCS has faster decompressing speed and lower approximation error when the compression ratio is small.

2. Background

2.1. Notations and basic tensor operations

Scalars, vectors, matrices and tensors are represented by lowercase, bold lowercase, bold capital and calligraphic letters respectively. Symbols “ $*$ ”, “ \circ ”, and “ \otimes ”, denote Hadamard product, vector outer product, and convolution, respectively. An N -th order tensor is rank-1 if it can be represented by the outer product of N vectors. Given a tensor $\mathcal{T} \in \mathbb{R}^{I_1 \times \dots \times I_N}$, its vectorization is denoted by $\text{vec}(\mathcal{T}) \in \mathbb{R}^{\prod_{n=1}^N I_n}$, its mode- n matricization of is denoted by $\mathbf{T}_{(n)} \in \mathbb{R}^{I_n \times \prod_{i \neq n} I_i}$. The Frobenius norm of \mathcal{T} is represented by $\|\mathcal{T}\|_F = \|\text{vec}(\mathcal{T})\|_F$. For any $N \in \mathbb{N}^+$, we denote $[N] := \{1, \dots, N\}$. For any two tensors \mathcal{M}, \mathcal{N} with the same size, their tensor inner product is denoted by $\langle \mathcal{M}, \mathcal{N} \rangle = \text{vec}(\mathcal{M})^T \text{vec}(\mathcal{N})$. The CPD of $\mathcal{T} \in \mathbb{R}^{I_1 \times \dots \times I_N}$ is a sum of rank-1 tensors, i.e. $\mathcal{T} \approx \sum_{r=1}^R \lambda_r \mathbf{u}_r^{(1)} \circ \dots \circ \mathbf{u}_r^{(N)} := [\boldsymbol{\lambda}; \mathbf{U}^{(1)}, \dots, \mathbf{U}^{(N)}]$, where R is the CP rank, $\boldsymbol{\lambda} \in \mathbb{R}^R$, $\mathbf{U}^{(n)} = [\mathbf{u}_1^{(n)}, \dots, \mathbf{u}_R^{(n)}] \in \mathbb{R}^{I_n \times R}$ for $n \in [N]$.

Given any two tensors $\mathcal{X} \in \mathbb{R}^{I_1 \times I_2 \times \dots \times I_P}$, $\mathcal{Y} \in \mathbb{R}^{J_1 \times J_2 \times \dots \times J_Q}$, their contraction is denoted and computed by $[\mathcal{X} \circledast \mathcal{Y}]_{\mathbb{L}} = \mathcal{X}_{\mathbb{P}} \mathcal{Y}_{\mathbb{Q}} = \sum_{\mathbb{O}} \mathcal{X}_{\cdot, \mathbb{O}} \otimes \mathcal{Y}_{\mathbb{O}, \cdot}$, where $\mathbb{P} := \{i_1 \times \dots \times i_P\}$ for $i_n \in [I_n]$, $\mathbb{Q} := \{j_1 \times \dots \times j_Q\}$ for $j_n \in [J_n]$, $\mathbb{O} = \mathbb{P} \cap \mathbb{Q}$ are the specified contraction indices, $\mathbb{L} = (\mathbb{P} \cup \mathbb{Q}) \setminus \mathbb{O}$ are the free indices, symbol “ \otimes ” denotes tensor product. When applied to two vectors or matrices, “ \otimes ” degrades to Kronecker product of them. Moreover, given two vectors \mathbf{u} and \mathbf{v} , we have $\text{vec}(\mathbf{u} \circ \mathbf{v}) = \mathbf{v} \otimes \mathbf{u}$. Given a series of matrices $\mathbf{M}_n \in \mathbb{R}^{I_n \times J_n}$ for $n \in [N]$, their contraction with a tensor $\mathcal{T} \in \mathbb{R}^{I_1 \times \dots \times I_N}$ is denoted and computed by $[\mathcal{T}(\mathbf{M}_1, \dots, \mathbf{M}_N)]_{j_1, \dots, j_N} = \sum_{i_1=1}^{I_1} \dots \sum_{i_N=1}^{I_N} \mathcal{T}_{i_1, \dots, i_N} \mathbf{M}_1(i_1, j_1) \dots \mathbf{M}_N(i_N, j_N)$ for $j_n \in [J_n]$. Specially, for a 3rd-order tensor $\mathcal{T} \in \mathbb{R}^{I \times I \times I}$ and a vector $\mathbf{u} \in \mathbb{R}^I$, $\mathcal{T}(\mathbf{u}, \mathbf{u}, \mathbf{u}) =$

$\langle \mathcal{T}, \mathbf{u} \circ \mathbf{u} \circ \mathbf{u} \rangle$, $\mathcal{T}(\mathbf{I}, \mathbf{u}, \mathbf{u})_i = \langle \mathcal{T}, \mathbf{e}_i \circ \mathbf{u} \circ \mathbf{u} \rangle$ where $\mathbf{I} \in \mathbb{R}^{I \times I}$ is the identity matrix, $\mathbf{e}_i \in \mathbb{R}^I$ is the i th standard basis vector.

2.2. Related works

In this section, we briefly introduce some sketching techniques that are closely related to our work.

Definition 1 (Count Sketch [19]): Let $\mathbf{h} : [I] \mapsto [J]$ and $\mathbf{s} : [I] \mapsto \{\pm 1\}$ be two 2-wise independent Hash functions. The CS of a vector $\mathbf{x} \in \mathbb{R}^I$ takes $O(\text{nnz}(\mathbf{x}))$ time [15] and produces a projection $\text{CS}(\mathbf{x}) \in \mathbb{R}^J$ with each element computed by:

$$\text{CS}(\mathbf{x}; \mathbf{h}, \mathbf{s})_j = \sum_{\mathbf{h}(i)=j} \mathbf{s}(i)\mathbf{x}(i). \quad (1)$$

When the input is a matrix $\mathbf{X} \in \mathbb{R}^{I \times K}$, CS can be applied on each column of \mathbf{X} and produces a matrix $\mathbf{Y} \in \mathbb{R}^{J \times K}$. Essentially, CS is a sketch for vectors.

Definition 2 (Tensor Sketch [20]): Given an N th-order tensor $\mathcal{T} \in \mathbb{R}^{I_1 \times \dots \times I_N}$, N pairs of 2-wise independent Hash functions $\mathbf{h}_n : [I_n] \mapsto [J]$, $\mathbf{s}_n : [I_n] \mapsto \{\pm 1\}$, $\text{TS}(\mathcal{T}) \in \mathbb{R}^J$ is computed in $O(\text{nnz}(\mathcal{T}))$ time by:

$$\text{TS}(\mathcal{T}; \{\mathbf{h}_n, \mathbf{s}_n\}_{n=1}^N)_j = \sum_{\mathcal{H}_{i_1, \dots, i_N} = j} \mathcal{S}_{i_1, \dots, i_N} \mathcal{T}_{i_1, \dots, i_N}, \quad (2)$$

where $\mathcal{H}_{i_1, \dots, i_N} = (\mathbf{h}_1(i_1) + \dots + \mathbf{h}_N(i_N) - N) \bmod J + 1$, \bmod denotes the modulo operator, $\mathcal{S}_{i_1, \dots, i_N} = \mathbf{s}_1(i_1)\mathbf{s}_2(i_2)\dots\mathbf{s}_N(i_N)$. Specially, when $\mathcal{T} \approx \sum_{r=1}^R \lambda_r \mathbf{u}_r^{(1)} \circ \dots \circ \mathbf{u}_r^{(N)} := \llbracket \boldsymbol{\lambda}; \mathbf{U}^{(1)}, \dots, \mathbf{U}^{(N)} \rrbracket$ is a CP rank- R tensor, $\text{TS}(\mathcal{T})$ can be computed by the mode- J circular convolution of the CS of each factor

vector as:

$$\begin{aligned} \text{TS}(\mathcal{T}; \{\mathbf{h}_n, \mathbf{s}_n\}_{n=1}^N) &= \sum_{r=1}^R \lambda_r \text{CS}_1(\mathbf{u}_r^{(1)}) \circledast_J \cdots \circledast_J \text{CS}_N(\mathbf{u}_r^{(N)}) \\ &= \sum_{r=1}^R \lambda_r \text{F}^{-1}(\text{F}(\text{CS}_1(\mathbf{U}^{(1)})(:, r)) * \cdots * \text{F}(\text{CS}_N(\mathbf{U}^{(N)})(:, r))), \end{aligned} \quad (3)$$

where $\text{CS}_n(\mathbf{U}^{(n)}) \in \mathbb{R}^{J \times R}$ is based on $(\mathbf{h}_n, \mathbf{s}_n)$ for $n \in [N]$, F and F^{-1} denote FFT and its inverse, respectively. By using FFT, (3) can be computed in $\mathcal{O}(\max_n \text{nnz}(\mathbf{U}^{(n)}) + R J \log J)$ time.

Definition 3 (Higher-order Count Sketch [29]): Given $\mathcal{T} \in \mathbb{R}^{I_1 \times \cdots \times I_N}$, N pairs of 2-wise independent Hash functions $\mathbf{h}_n : [I_n] \mapsto [J_n]$, $\mathbf{s}_n : [I_n] \mapsto \{\pm 1\}$, $\text{HCS}(\mathcal{T}) \in \mathbb{R}^{J_1 \times \cdots \times J_N}$ is computed by

$$\text{HCS}(\mathcal{T}; \{\mathbf{h}_n, \mathbf{s}_n\}_{n=1}^N)_{j_1, \dots, j_N} = \sum_{\substack{\mathbf{h}_1(i_1)=j_1 \\ \vdots \\ \mathbf{h}_N(i_N)=j_N}} \mathcal{S}_{i_1, \dots, i_N} \mathcal{T}_{i_1, \dots, i_N}, \quad (4)$$

where $\mathcal{S}_{i_1, \dots, i_N}$ is defined the same as in (2). The computational complexity of (4) is $\mathcal{O}(\text{nnz}(\mathcal{T}))$. When $\mathcal{T} \approx \sum_{r=1}^R \lambda_r \mathbf{u}_r^{(1)} \circ \cdots \circ \mathbf{u}_r^{(N)} = \llbracket \boldsymbol{\lambda}; \mathbf{U}^{(1)}, \dots, \mathbf{U}^{(N)} \rrbracket \in \mathbb{R}^{I_1 \times \cdots \times I_N}$ is a CP rank- R tensor, $\text{HCS}(\mathcal{T})$ can be computed by

$$\text{HCS}(\mathcal{T}; \{\mathbf{h}_n, \mathbf{s}_n\}_{n=1}^N) = \sum_{r=1}^R \lambda_r \text{CS}_1(\mathbf{U}^{(1)})(:, r) \circ \cdots \circ \text{CS}_N(\mathbf{U}^{(N)})(:, r). \quad (5)$$

Notice that the vector outer product should be materialized when $R > 1$. Hence, the computational complexity of (5) is $\mathcal{O}(\max_n \text{nnz}(\mathbf{U}^{(n)}) + R \prod_{n=1}^N J_n)$.

3. The proposed method

As noticed in Section 2, HCS sketches an input tensor into a lower-dimensional one. Therefore, the multi-dimensional structure information can be well preserved. However, for CP rank- R tensors, HCS computes the outer product of CS of each factor vector, which is much slower than TS. Below we will propose FCS, which can achieve a balance between the approximation accuracy and computational complexity.

Definition 4 (Fast Count Sketch): Given $\mathcal{T} \in \mathbb{R}^{I_1 \times \dots \times I_N}$, N pairs of 2-wise independent Hash functions $\mathbf{h}_n : [I_n] \mapsto [J_n]$, $\mathbf{s}_n : [I_n] \mapsto \{\pm 1\}$, $\text{FCS}(\mathcal{T}) \in \mathbb{R}^{\tilde{J}}$ is defined as:

$$\text{FCS}(\mathcal{T}; \{\mathbf{h}_n, \mathbf{s}_n\}_{n=1}^N) := \text{CS}(\text{vec}(\mathcal{T}); \mathbf{h}_{N+1}, \mathbf{s}_{N+1}), \quad (6)$$

where $\tilde{J} = \sum_{n=1}^N J_n - N + 1$. $\mathbf{h}_{N+1} : [\tilde{I}] \mapsto [\tilde{J}]$ and $\mathbf{s}_{N+1} : [\tilde{I}] \mapsto \{\pm 1\}$ ($\tilde{I} = \prod_{n=1}^N I_n$) satisfy:

$$\begin{aligned} \mathbf{s}_{N+1} \left(\sum_{n=1}^N (i_n - 1) \prod_{j=1}^{n-1} I_j + 1 \right) &= \prod_{n=1}^N \mathbf{s}_n(i_n) \\ \mathbf{h}_{N+1} \left(\sum_{n=1}^N (i_n - 1) \prod_{j=1}^{n-1} I_j + 1 \right) &= \sum_{n=1}^N \mathbf{h}_n(i_n) - N + 1. \end{aligned} \quad (7)$$

As it does in (6), FCS on the original tensor equals multiple shorter Hash functions based CS on the vectorized tensor.

In the next subsections, we will present the computation details of FCS for the CP rank- R tensor and the general tensor.

3.1. CP rank-R tensor

Consider the case where \mathcal{T} admits CPD $\mathcal{T} = \sum_{r=1}^R \lambda_r \mathbf{u}_r^{(1)} \circ \dots \circ \mathbf{u}_r^{(N)} = \llbracket \boldsymbol{\lambda}; \mathbf{U}^{(1)}, \dots, \mathbf{U}^{(N)} \rrbracket \in \mathbb{R}^{I_1 \times \dots \times I_N}$. Given N pairs of 2-wise independent Hash functions $\mathbf{h}_n : [I_n] \mapsto [J_n]$ and $\mathbf{s}_n : [I_n] \mapsto \{\pm 1\}$, $\text{FCS}(\mathcal{T})$ is computed by

$$\begin{aligned} \text{FCS}(\mathcal{T}; \{\mathbf{h}_n, \mathbf{s}_n\}_{n=1}^N) &= \text{CS}\left(\sum_{r=1}^R \lambda_r \bigotimes_{n=N}^1 (\mathbf{u}_r^{(n)}); \mathbf{h}_{N+1}, \mathbf{s}_{N+1}\right) \\ &= \sum_{r=1}^R \lambda_r \text{CS}_1(\mathbf{U}^{(1)})(:, r) \otimes \dots \otimes \text{CS}_N(\mathbf{U}^{(N)})(:, r) \\ &= \sum_{r=1}^R \lambda_r \text{F}^{-1}(\text{F}(\text{CS}_1(\mathbf{U}^{(1)})(:, r), \tilde{\mathcal{J}}) * \dots * \text{F}(\text{CS}_N(\mathbf{U}^{(N)})(:, r), \tilde{\mathcal{J}})), \end{aligned} \quad (8)$$

where $\bigotimes_{n=N}^1 (\mathbf{u}_r^{(n)}) := \mathbf{u}_r^{(N)} \otimes \mathbf{u}_r^{(N-1)} \otimes \dots \otimes \mathbf{u}_r^{(1)}$, $\text{F}(\cdot, \tilde{\mathcal{J}})$ and $\text{F}^{-1}(\cdot, \tilde{\mathcal{J}})$ denote zero-padded $\tilde{\mathcal{J}}$ -point FFT and its inverse. The proof of (8) is as follows:

Proof (proof of (8)). *Given a rank-1 tensor $\mathcal{T} = \mathbf{u}^{(1)} \circ \mathbf{u}^{(2)} \circ \dots \circ \mathbf{u}^{(N)} \in \mathbb{R}^{I_1 \times I_2 \times \dots \times I_N}$, if we assign $l = \sum_{n=1}^N (i_n - 1) \prod_{j=1}^{n-1} I_j + 1$, then $\text{vec}(\mathcal{T})_l = \mathbf{u}_{i_1}^{(1)} \dots \mathbf{u}_{i_N}^{(N)}$. We have*

$$\begin{aligned} &\sum_{i_1=1}^{I_1} \dots \sum_{i_N=1}^{I_N} \text{vec}(\mathcal{T})_l \mathbf{s}_1(i_1) \dots \mathbf{s}_N(i_N) \mathbf{w}^{\mathbf{h}_1(i_1) + \dots + \mathbf{h}_N(i_N) - N} \\ &= \sum_{i_1=1}^{I_1} \dots \sum_{i_N=1}^{I_N} \mathbf{u}_{i_1}^{(1)} \dots \mathbf{u}_{i_N}^{(N)} \mathbf{s}_1(i_1) \dots \mathbf{s}_N(i_N) \mathbf{w}^{\mathbf{h}_1(i_1) + \dots + \mathbf{h}_N(i_N) - N} \\ &= \sum_{i_1} \mathbf{u}_{i_1}^{(1)} \mathbf{s}_1(i_1) \mathbf{w}^{\mathbf{h}_1(i_1) - 1} \dots \sum_{i_N} \mathbf{u}_{i_N}^{(N)} \mathbf{s}_N(i_N) \mathbf{w}^{\mathbf{h}_N(i_N) - 1} \\ &= \mathcal{P}_{\text{CS}_1(\mathbf{u}^{(1)})}(\mathbf{w}) \dots \mathcal{P}_{\text{CS}_N(\mathbf{u}^{(N)})}(\mathbf{w}), \end{aligned} \quad (9)$$

where \mathbf{w} is a symbolic variable, $\mathcal{P}_{\text{CS}_n(\mathbf{u}^{(n)})}(\mathbf{w})$ is the polynomial form of $\text{CS}_n(\mathbf{u}^{(n)})$

for $n \in [N]$. Let $\mathbf{s}_{N+1}(l) = \mathbf{s}_1(i_1) \cdots \mathbf{s}_N(i_N)$, $\mathbf{h}_{N+1}(l) = \mathbf{h}_1(i_1) + \cdots + \mathbf{h}_N(i_N) - N + 1$, we have

$$\begin{aligned}
& \sum_{i_1=1}^{I_1} \cdots \sum_{i_N=1}^{I_N} \text{vec}(\mathcal{T})_l \mathbf{s}_1(i_1) \cdots \mathbf{s}_N(i_N) \mathbf{w}^{\mathbf{h}_1(i_1) + \cdots + \mathbf{h}_N(i_N) - N} \\
&= \sum_l \text{vec}(\mathcal{T})_l \mathbf{s}_{N+1}(l) \mathbf{w}^{\mathbf{h}_{N+1}(l) - 1} \\
&= \mathcal{P}_{\text{CS}(\text{vec}(\mathcal{T}); \mathbf{h}_{N+1}, \mathbf{s}_{N+1})}(\mathbf{w}) := \mathcal{P}_{\text{FCS}(\mathcal{T}; \{\mathbf{h}_n, \mathbf{s}_n\}_{n=1}^N)}(\mathbf{w}).
\end{aligned} \tag{10}$$

Therefore,

$$\mathcal{P}_{\text{FCS}(\mathcal{T}; \{\mathbf{h}_n, \mathbf{s}_n\}_{n=1}^N)}(\mathbf{w}) = \mathcal{P}_{\text{CS}_1(\mathbf{u}^{(1)})}(\mathbf{w}) \cdots \mathcal{P}_{\text{CS}_N(\mathbf{u}^{(N)})}(\mathbf{w}). \tag{11}$$

Due to the fact that polynomial multiplication equals the convolution of their coefficients, we have

$$\begin{aligned}
\text{FCS}(\mathcal{T}; \{\mathbf{h}_n, \mathbf{s}_n\}_{n=1}^N) &= \text{CS}_1(\mathbf{u}^{(1)}) \otimes \cdots \otimes \text{CS}_N(\mathbf{u}^{(N)}) \\
&= \mathbb{F}^{-1}(\mathbb{F}(\text{CS}_1(\mathbf{u}^{(1)})) * \cdots * \mathbb{F}(\text{CS}_N(\mathbf{u}^{(N)}))).
\end{aligned} \tag{12}$$

Based on the linearity, the conclusion applies to CP rank- R tensors immediately, which completes the proof.

The computational complexity of (8) is $O(\max_n \text{nnz}(\mathbf{U}^{(n)}) + R\tilde{J} \log \tilde{J})$, which is asymptotically identical to TS for low-order tensors, and is much faster than the vector outer product of HCS shown in (5). Since the vectorization form of the CPD is equivalent to the original form after reordering the elements, the multi-dimensional structure of the original tensor can be well preserved.

3.2. General tensor

For most real-world low-rank tensor data, the rank-1 factors cannot be known in advance. FCS for general tensors can be computed in $O(\text{nnz}(\mathcal{T}))$ time by:

$$\begin{aligned} \text{FCS}(\mathcal{T}; \{\mathbf{h}_n, \mathbf{s}_n\}_{n=1}^N)_j &= \sum_{\mathbf{h}_{N+1}(i)=j}^{\tilde{I}} \mathbf{s}_{N+1}(i) * \text{vec}(\mathcal{T})_i \\ &= \sum_{\mathcal{H}_{i_1, \dots, i_N}=j} \mathcal{S}_{i_1, \dots, i_N} \mathcal{T}_{i_1, \dots, i_N}, \end{aligned} \quad (13)$$

where $\mathcal{H}_{i_1, \dots, i_N} = \mathbf{h}_1(i_1) + \dots + \mathbf{h}_N(i_N) - N + 1$, $\mathcal{S}_{i_1, \dots, i_N} = \mathbf{s}_1(i_1)\mathbf{s}_2(i_2) \cdots \mathbf{s}_N(i_N)$ for $j \in [\tilde{J}]$. Notice that \mathcal{H} and \mathcal{S} are not necessarily explicitly built so that the only $\{\mathbf{h}_n, \mathbf{s}_n\}_{n=1}^N$ are required to be stored.

We summarize the main differences of FCS among CS, TS, and HCS below:

- (1) Compared with CS which applies on $\text{vec}(\mathcal{T})$, FCS is based on multiple shorter Hash function pairs $\{\mathbf{h}_n, \mathbf{s}_n\}_{n=1}^N$, while CS generates a long Hash function pair $\mathbf{h} : [\tilde{I}] \mapsto [\tilde{J}]$ and $\mathbf{s} : [\tilde{I}] \mapsto \{\pm 1\}$ to match the dimensionality of $\text{vec}(\mathcal{T})$. Therefore, only $\{\mathbf{h}_n, \mathbf{s}_n\}_{n=1}^N$ are stored for FCS, which reduces the storage complexity from $O(\tilde{I})$ to $O(\sum_{n=1}^N I_n)$. Besides, as shown in (8), FCS for CP rank- R tensors can be computed by FFT, which accelerates the original CS.
- (2) Compared with TS, FCS avoids the modular operation in (2) and (3). Intuitively, the multiple Hash functions of FCS are integrated in a way that the spatial structure of the input tensor can be preserved more sufficiently, while the modular operation in TS breaks the spatial relationship

of tensors. We will show that FCS provides a more accurate estimator for tensor inner product than TS under the same Hash functions in Proposition 1.

- (3) Compared with HCS, the vector outer product in (5) is also avoided. Besides, as shown in Table 1, the approximation for $\mathcal{T}(\mathbf{I}, \mathbf{u}, \mathbf{u})$ and $\mathcal{T}(\mathbf{u}, \mathbf{u}, \mathbf{u})$ by FCS is more efficient than HCS under the same Hash length. Finally, we will show in the experiments that FCS has faster decompressing time than HCS for Kronecker product and tensor contraction compression.

3.3. Tensor contraction approximation

We approximate two specific tensor contractions $\mathcal{T}(\mathbf{u}, \mathbf{u}, \mathbf{u})$ and $\mathcal{T}(\mathbf{I}, \mathbf{u}, \mathbf{u})$ using FCS. For brevity, we omit the Hash function pairs in (2) and (6). The following proposition states the validity of the approximation:

Proposition 1: For any two tensors $\mathcal{M}, \mathcal{N} \in \mathbb{R}^{I_1 \times I_2 \times I_3}$, $\langle \text{FCS}(\mathcal{M}), \text{FCS}(\mathcal{N}) \rangle$ provides a consistent estimator of $\langle \mathcal{M}, \mathcal{N} \rangle$ with the variance satisfying

$$V_{\mathbf{h}, \mathbf{s}}[\langle \text{FCS}(\mathcal{M}), \text{FCS}(\mathcal{N}) \rangle] \leq V_{\mathbf{h}, \mathbf{s}}[\langle \text{TS}(\mathcal{M}), \text{TS}(\mathcal{N}) \rangle], \quad (14)$$

if the Hash functions for TS and FCS are equalized. The validity is guaranteed from two aspects: the consistency guarantees the approximation is feasible, and (14) illustrates FCS computes a more accurate estimator for tensor inner product than TS [7]. The proof is deferred to the supplementary materials due to space limit.

Based on Proposition 1, the following corollary gives the approximation error:

Corollary 1: Given any 3rd-order tensor $\mathcal{T} \in \mathbb{R}^{I \times I \times I}$, unit vector $\mathbf{u} \in \mathbb{R}^I$,

from Chebychev’s inequality, if we run the sketch $D = \Omega(\log(1/\delta))$ times, then for any $\epsilon > 0$, with probability at least $1 - \delta$ we have

$$\begin{aligned} \mathbb{P}_{\mathbf{h},s}[|\langle \text{FCS}(\mathcal{T}), \text{FCS}(\mathbf{u} \circ \mathbf{u} \circ \mathbf{u}) \rangle - \mathcal{T}(\mathbf{u}, \mathbf{u}, \mathbf{u})| \geq \epsilon] &\leq O\left(\frac{\|\mathcal{T}\|_{\text{F}}^2}{J\epsilon^2}\right) \\ \mathbb{P}_{\mathbf{h},s}[|\langle \text{FCS}(\mathcal{T}), \text{FCS}(\mathbf{e}_i \circ \mathbf{u} \circ \mathbf{u}) \rangle - \mathcal{T}(\mathbf{e}_i, \mathbf{u}, \mathbf{u})| \geq \epsilon] &\leq O\left(\frac{\|\mathcal{T}\|_{\text{F}}^2}{J\epsilon^2}\right), \end{aligned} \quad (15)$$

where the symbol \mathbb{P} stands for probability. The Hash lengths of all Hash functions are set to J for simplicity. The proof can be found in the supplementary materials.

4. Experiments

In this section, we verify the effectiveness of the proposed FCS by comparing it with CS, TS and HCS in various numerical experiments, including CPD, TRN compression, the Kronecker product and tensor contraction compression. To make the estimation more robust, we compute D number of independent sketches and return the median for all sketching methods.

4.1. CP decomposition

We consider two CPD algorithms dubbed RTPM and ALS which involve $\mathcal{T}(\mathbf{u}, \mathbf{u}, \mathbf{u})$ and $\mathcal{T}(\mathbf{I}, \mathbf{u}, \mathbf{u})$. From Corollary 1, the two tensor contractions can be approximated by:

$$\begin{aligned} \mathcal{T}(\mathbf{u}, \mathbf{u}, \mathbf{u}) &\approx \langle \text{FCS}(\mathcal{T}), \text{FCS}(\mathbf{u} \circ \mathbf{u} \circ \mathbf{u}) \rangle \\ &= \langle \text{FCS}(\mathcal{T}), \text{F}^{-1}(\text{F}(\text{CS}_1(\mathbf{u})) * \text{F}(\text{CS}_2(\mathbf{u})) * \text{F}(\text{CS}_3(\mathbf{u}))) \rangle \end{aligned} \quad (16)$$

$$\begin{aligned}
\mathcal{T}(\mathbf{I}, \mathbf{u}, \mathbf{u})_i &\approx \langle \text{FCS}(\mathcal{T}), \text{FCS}(\mathbf{e}_i \circ \mathbf{u} \circ \mathbf{u}) \rangle \\
&= \left\langle \text{F}^{-1}(\text{F}(\text{FCS}(\mathcal{T})) * \overline{\text{F}(\text{CS}_2(\mathbf{u}))} * \overline{\text{F}(\text{CS}_3(\mathbf{u}))}), \text{CS}_1(\mathbf{e}_i) \right\rangle \quad (17) \\
&:= \langle \mathbf{z}, \text{CS}_1(\mathbf{e}_i) \rangle = \mathbf{s}_1(i) \mathbf{z}(\mathbf{h}_1(i)).
\end{aligned}$$

(17) holds due to the unitary property of FFT. Both $\text{FCS}(\mathcal{T})$ and \mathbf{z} are irrelevant to i and can be computed beforehand. We summarize the computational and storage complexity of RTPM and ALS with and without sketching (which we term “plain”) in Table 1. All Hash lengths are set to J for simplicity.

Table 1: Computational and storage complexity of the plain, CS, TS, HCS, and FCS based RTPM and ALS for a 3rd-order tensor $\mathcal{T} \in \mathbb{R}^{I \times I \times I}$. R denotes the target CP rank.

RTPM/ALS	plain	CS	TS	HCS	FCS
preprocessing and sketch building for $\mathcal{T}=[\lambda; \mathbf{U}, \mathbf{U}, \mathbf{U}]$	$O(RI^3)$	$O(RI^3 + \text{nnz}(\mathcal{T}))$	$O(\text{nnz}(\mathbf{U}) + RJ \log J)$	$O(\text{nnz}(\mathbf{U}) + RJ^3)$	$O(\text{nnz}(\mathbf{U}) + RJ \log J)$
preprocessing and sketch building for general tensor \mathcal{T}	-	$O(\text{nnz}(\mathcal{T}))$	$O(\text{nnz}(\mathcal{T}))$	$O(\text{nnz}(\mathcal{T}))$	$O(\text{nnz}(\mathcal{T}))$
$\mathcal{T}(\mathbf{I}, \mathbf{u}, \mathbf{u})$ or its approximation	$O(I^3)$	$O(\text{nnz}(\mathbf{u})^2 I)$	$O(\text{nnz}(\mathbf{u}) + J \log J + J)$	$O(\text{nnz}(\mathbf{u}) + IJ^2)$	$O(\text{nnz}(\mathbf{u}) + J \log J + I)$
$\mathcal{T}(\mathbf{u}, \mathbf{u}, \mathbf{u})$ or its approximation	$O(I^3)$	$O(\text{nnz}(\mathbf{u})^3)$	$O(\text{nnz}(\mathbf{u}) + J \log J)$	$O(\text{nnz}(\mathbf{u}) + J^3)$	$O(\text{nnz}(\mathbf{u}) + J \log J)$
storage for Hash functions	-	$O(I^3)$	$O(I)$	$O(I)$	$O(I)$

4.1.1. Robust tensor power method

RTPM decomposes a noisy input tensor into rank-1 components with orthogonal basis vectors. For each rank-1 factor, it computes power iteration $\mathbf{u} = \frac{\mathcal{T}(\mathbf{I}, \mathbf{u}, \mathbf{u})}{\|\mathcal{T}(\mathbf{I}, \mathbf{u}, \mathbf{u})\|_{\text{F}}}$ from random initializations and obtains the eigenvalue by $\mathcal{T}(\mathbf{u}, \mathbf{u}, \mathbf{u})$.

It is necessary to note that most real-world low-rank tensor data are asymmetric. The power iteration of asymmetric RTPM can be performed similarly as the symmetric case via alternating rank-1 update [34]. By (13), we can accelerate RTPM on real-world data using FCS.

The effectiveness of FCS is verified by accelerating RTPM on synthetic

and real-world datasets. For the synthetic case, we generate a symmetric CP rank-10 tensor $\mathcal{T} = \sum_{r=1}^{10} \mathbf{u}_r \circ \mathbf{u}_r \circ \mathbf{u}_r \in \mathbb{R}^{100 \times 100 \times 100}$, where $\{\mathbf{u}_r\}_{r=1}^{10}$ forms a random orthonormal basis. \mathcal{T} is then perturbed by zero-mean Gaussian noise with standard deviation $\sigma = 0.01$. The number of independent sketches D , initial vectors L and power iterations T are set to 2, 15 and 20, respectively. The Hash functions for TS and FCS are equalized to produce identical initializations. We choose residual norm as the performance metric.

We compare the performance of FCS against the plain, CS, and TS based RTPM with the Hash lengths ranging from 1000 to 10000, and the results are shown in Fig. 1. Clearly, FCS-RTPM achieves better approximation accuracy than CS- and TS- RTPM. Although FCS-RTPM is slower than TS-RTPM, it is still much faster than the CS- and plain RTPM under most Hash lengths. Notice that CS-RTPM is even slower than the plain RTPM, hence we do not compare it with FCS-RTPM in the real-world experiment.

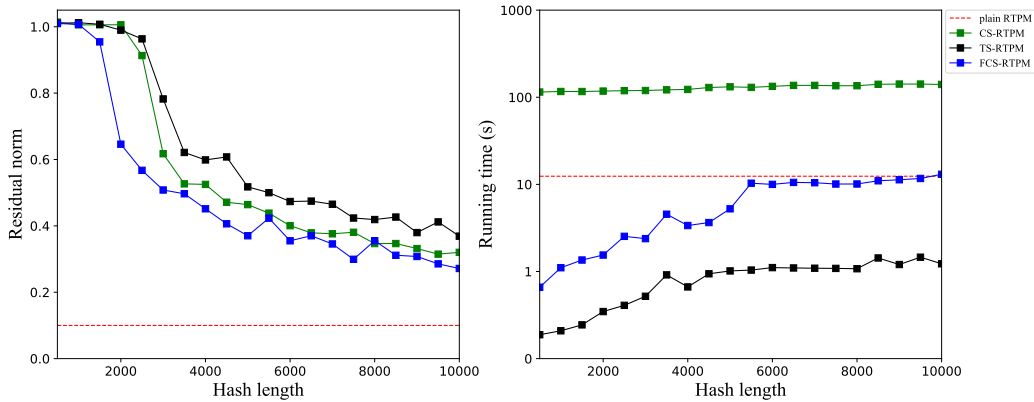


Figure 1: Performance comparison on a synthetic symmetric CP rank-10 tensor $\mathcal{T} \in \mathbb{R}^{100 \times 100 \times 100}$ for plain, CS, TS and FCS based RTPM.

We compare the performance of HCS and FCS based RTPM on a synthetic symmetric CP rank-10 tensor $\mathcal{T} \in \mathbb{R}^{50 \times 50 \times 50}$. Denote the Hash lengths

of HCS and FCS as J_1 and J_2 , respectively. Given a 3rd-order tensor with dimension I , J_1 should be smaller than I to sketch the tensor into a lower dimensional one. However, the sketched dimension for FCS requires to be $O(I^3)$ for provable approximation [7]. As a result, it is not fair to set $J_1 \approx J_2$ in this experiment. Therefore we choose J_1 and J_2 such that the sketched dimensions are similar ($J_1^3 \approx 3J_2 - 2$). The experiment results are displayed in Table 2. It can be seen that FCS beats HCS in terms of approximation accuracy and running speed under various Hash lengths, noise intensities, and number of independent sketches.

Table 2: Performance comparison on a synthetic symmetric CP rank-10 tensor $\mathcal{T} \in \mathbb{R}^{50 \times 50 \times 50}$ by HCS and FCS based RTPM under similar sketched dimension.

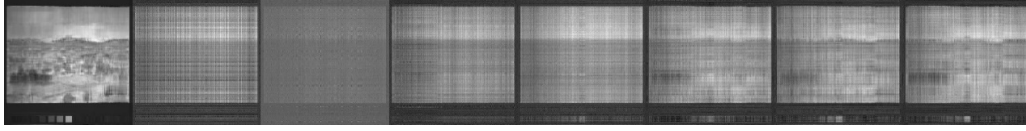
σ	Residual norm						Running time (s)						
	J_1	14	18	21	23	25	14	18	21	23	25		
0.01	HCS-RTPM	$D = 10$	1.3020	0.8305	0.7744	0.7727	0.7719	12.2329	30.7566	46.7719	58.4108	67.7999	
		$D = 15$	0.8237	0.6583	0.6089	0.5938	0.5699	18.2351	45.5026	70.3092	88.6696	104.4252	
		$D = 20$	0.6904	0.6702	0.5229	0.4738	0.4733	24.5617	63.1505	95.1202	119.8723	140.5284	
	FCS-RTPM	J_2	200	250	300	350	400	200	250	300	350	400	
		$D = 10$	0.3304	0.2033	0.1701	0.1525	0.1375	4.9459	8.8239	16.7354	21.9275	28.4605	
		$D = 15$	0.2440	0.1794	0.1472	0.1280	0.1179	6.9054	13.9064	26.1508	34.1260	42.7100	
		$D = 20$	0.2135	0.1544	0.1226	0.1050	0.0899	8.7913	18.2077	34.4879	44.7941	56.2395	
	0.1	HCS-RTPM	J_1	14	18	21	23	25	14	18	21	23	25
			$D = 10$	0.8941	0.8414	0.7493	0.6796	0.6334	12.1630	28.7772	42.9283	54.9871	65.9807
$D = 15$			0.7692	0.6618	0.6112	0.5766	0.5738	18.0038	43.0994	65.3426	85.6515	103.2082	
FCS-RTPM		$D = 20$	0.6814	0.6155	0.5256	0.4697	0.5409	24.2827	57.0479	88.6810	122.2182	149.7220	
		J_2	200	250	300	350	400	200	250	300	350	400	
		$D = 10$	0.3123	0.2052	0.1648	0.1386	0.1277	4.8647	8.7281	16.5311	21.5956	28.6445	
		$D = 15$	0.2613	0.1665	0.1568	0.1289	0.1063	6.8684	14.6268	27.2106	35.0255	44.4975	
		$D = 20$	0.2102	0.1550	0.1173	0.0987	0.0939	8.9151	18.8304	34.3682	48.4351	59.3935	

For the real-world data based experiment, we compute the plain, TS and FCS based RTPM using the same Hash functions on a hyperspectral imaging (HSI) dataset Watercolors and a light field dataset Buddha. Below we briefly introduce the two datasets and the preprocessing methods:

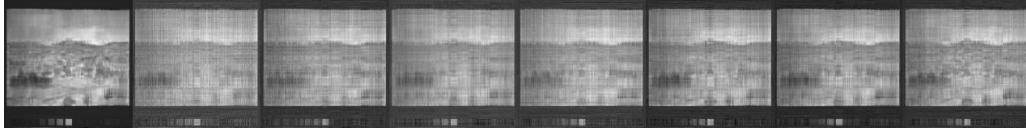
- (1) The Watercolors is a HSI dataset captured by a resolution $512 \times 512 \times 3$ cooled CCD camera with the wevelength ranging from 400 to 700 nm at the interval of 10 (31 bands in total) [35]. We transform the raw images to gray scale images and represent them as a $512 \times 512 \times 31$ tensor. The target CP rank is set as 15.
- (2) The Buddha dataset is captured by a resolution $768 \times 768 \times 3$ camera at 9×9 views [36]. Therefore, the raw data can be represented by a $768 \times 768 \times 3 \times 9 \times 9$ tensor. We transform the raw images to gray scale images, and resize them as a $192 \times 192 \times 81$ tensor. The target CP rank is set as 30.

We vary the compared Hash lengths from 5000 to 8000. The number of independent sketches D is set as 10 and 15, respectively. We choose peak signal to noise ratio (PSNR) as the performance metric. We display the 31st frame of the approximation results of Watercolors in Fig. 2 and the 1st frame of the approximation results of Buddha in Fig. 3, respectively. Clearly FCS-RTPM achieves better approximation quality than TS, especially when the Hash length is small. Although FCS-RTPM is slower than TS-RTPM, it is much faster than the plain RTPM.

$D = 10$

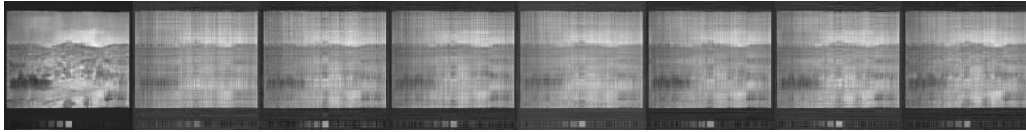


plain	TS (J=5000)	TS (J=5500)	TS (J=6000)	TS (J=6500)	TS (J=7000)	TS (J=7500)	TS (J=8000)
PSNR: 24.6191	PSNR: 12.0841	PSNR: 16.6650	PSNR: 18.6234	PSNR: 18.7716	PSNR: 19.6501	PSNR: 20.0508	PSNR: 20.3342
time: 1.7136e3	time: 4.9561	time: 5.5744	time: 6.0234	time: 6.1096	time: 8.2208	time: 7.7654	time: 7.9278

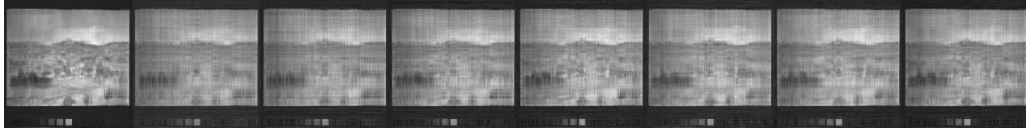


plain	FCS (J=5000)	FCS (J=5500)	FCS (J=6000)	FCS (J=6500)	FCS (J=7000)	FCS (J=7500)	FCS (J=8000)
PSNR: 24.6191	PSNR: 17.2813	PSNR: 20.7769	PSNR: 20.9595	PSNR: 21.0005	PSNR: 21.4534	PSNR: 21.5296	PSNR: 21.9185
time: 1.7136e3	time: 40.2463	time: 54.2101	time: 59.8770	time: 64.9402	time: 65.0799	time: 59.5772	time: 60.3623

$D = 15$



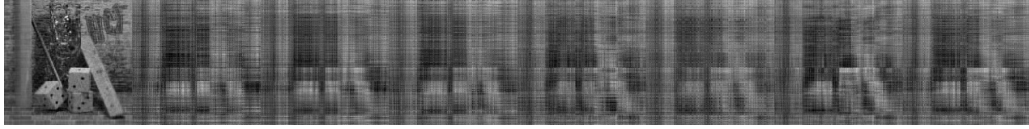
plain	TS (J=5000)	TS (J=5500)	TS (J=6000)	TS (J=6500)	TS (J=7000)	TS (J=7500)	TS (J=8000)
PSNR: 24.6191	PSNR: 19.9443	PSNR: 20.2582	PSNR: 20.6025	PSNR: 20.6217	PSNR: 20.8829	PSNR: 21.2371	PSNR: 21.2471
time: 1.7136e3	time: 8.0816	time: 9.0506	time: 9.7752	time: 10.6465	time: 11.4166	time: 12.0150	time: 12.2282



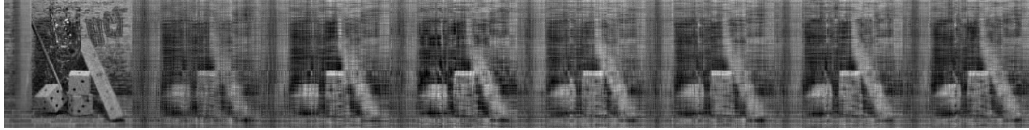
plain	FCS (J=5000)	FCS (J=5500)	FCS (J=6000)	FCS (J=6500)	FCS (J=7000)	FCS (J=7500)	FCS (J=8000)
PSNR: 24.6191	PSNR: 21.3232	PSNR: 21.4504	PSNR: 21.8326	PSNR: 22.1756	PSNR: 21.9244	PSNR: 22.2421	PSNR: 22.3577
time: 1.7136e3	time: 61.8661	time: 91.1924	time: 82.1203	time: 99.8431	time: 98.8338	time: 91.0331	time: 92.0321

Figure 2: Rank-15 approximation of TS-RTPM and FCS-RTPM on HSI dataset Watercolors. PSNR (dB) and running time (s) are tagged under each approximation figure.

$D = 10$

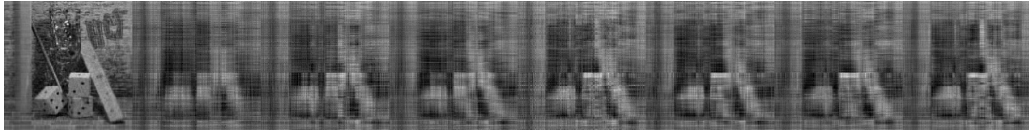


plain	TS (J=5000)	TS (J=5500)	TS (J=6000)	TS (J=6500)	TS (J=7000)	TS (J=7500)	TS (J=8000)
PSNR: 25.9897	PSNR: 17.4887	PSNR: 17.7042	PSNR: 17.7401	PSNR: 18.0425	PSNR: 18.2881	PSNR: 18.5143	PSNR: 18.6770
time: 1.0177e3	time: 9.5307	time: 9.5307	time: 9.530	time: 9.5307	time: 15.0014	time: 15.4034	time: 15.7005



plain	FCS (J=5000)	FCS (J=5500)	FCS (J=6000)	FCS (J=6500)	FCS (J=7000)	FCS (J=7500)	FCS (J=8000)
PSNR: 25.9897	PSNR: 18.8751	PSNR: 19.1553	PSNR: 19.4764	PSNR: 19.5203	PSNR: 19.6091	PSNR: 19.8708	PSNR: 19.8539
time: 1.0177e3	time: 80.0846	time: 119.9084	time: 106.3993	time: 130.2928	time: 128.0220	time: 117.8994	time: 118.4621

$D = 15$



plain	TS (J=5000)	TS (J=5500)	TS (J=6000)	TS (J=6500)	TS (J=7000)	TS (J=7500)	TS (J=8000)
PSNR: 25.9897	PSNR: 17.9567	PSNR: 18.4730	PSNR: 18.6564	PSNR: 18.9755	PSNR: 19.1599	PSNR: 19.0142	PSNR: 19.4703
time: 1.0177e3	time: 16.3893	time: 18.3014	time: 19.8582	time: 21.1023	time: 22.4747	time: 23.5413	time: 24.3670



plain	FCS (J=5000)	FCS (J=5500)	FCS (J=6000)	FCS (J=6500)	FCS (J=7000)	FCS (J=7500)	FCS (J=8000)
PSNR: 25.9897	PSNR: 19.6313	PSNR: 19.7102	PSNR: 19.7996	PSNR: 20.0785	PSNR: 20.2221	PSNR: 20.2445	PSNR: 20.7793
time: 1.0177e3	time: 121.6104	time: 181.2024	time: 160.3867	time: 197.0279	time: 193.3989	time: 179.3304	time: 180.1784

Figure 3: Rank-30 approximation of TS-RTPM and FCS-RTPM on light field dataset Buddha. PSNR (dB) and running time (s) are tagged under each approximation figure.

4.1.2. Alternating least squares

ALS is another efficient method for CPD, which requires computing [7]

$$\begin{aligned}
 \mathbf{T}_{(1)}(\mathbf{C} \odot \mathbf{B}) &= [\mathcal{T}(\mathbf{I}, \mathbf{b}_1, \mathbf{c}_1), \dots, \mathcal{T}(\mathbf{I}, \mathbf{b}_N, \mathbf{c}_N)] \\
 \mathbf{T}_{(2)}(\mathbf{A} \odot \mathbf{C}) &= [\mathcal{T}(\mathbf{c}_1, \mathbf{I}, \mathbf{a}_1), \dots, \mathcal{T}(\mathbf{c}_N, \mathbf{I}, \mathbf{a}_N)] \\
 \mathbf{T}_{(3)}(\mathbf{B} \odot \mathbf{A}) &= [\mathcal{T}(\mathbf{a}_1, \mathbf{b}_1, \mathbf{I}), \dots, \mathcal{T}(\mathbf{a}_N, \mathbf{b}_N, \mathbf{I})],
 \end{aligned} \tag{18}$$

iteratively. Hence we can approximate them like (17). In the experiment, we generate a synthetic asymmetric CP rank-10 tensor $\mathcal{T} = \sum_{r=1}^{10} \mathbf{u}_r \circ \mathbf{v}_r \circ \mathbf{w}_r \in \mathbb{R}^{400 \times 400 \times 400}$ as illustrated in the last subsection. We compare the plain, TS and FCS based ALS using the same Hash functions and the results are shown in Table 3. Clearly FCS is more accurate than TS under various conditions. Notice that as the Hash length gets smaller, the accuracy gap between TS and FCS gets bigger, and the speed gap gets smaller.

Table 3: Performance comparison on a synthetic asymmetric CP rank-10 tensor $\mathcal{T} \in \mathbb{R}^{400 \times 400 \times 400}$ by plain, TS and FCS based ALS.

σ	J	Residual norm					Running time (s)					
		3000	4000	5000	6000	7000	3000	4000	5000	6000	7000	
0.01	TS-ALS	$D = 10$	1.1898	0.9063	0.7684	0.6888	0.6198	16.0213	15.9789	15.9756	16.6813	16.9187
		$D = 15$	0.9721	0.7961	0.6981	0.6272	0.5763	16.358	16.4966	17.2223	17.4917	17.8075
		$D = 20$	0.6959	0.5899	0.5179	0.4684	0.4337	16.4243	17.3973	17.664	17.9625	18.3088
	FCS-ALS	$D = 10$	0.7801	0.6429	0.5618	0.4915	0.4547	18.3248	19.6939	20.9603	23.3214	24.7461
		$D = 15$	0.6949	0.5851	0.5168	0.4643	0.4311	20.2062	22.2532	23.453	26.2442	28.9429
		$D = 20$	0.5122	0.4342	0.3877	0.351	0.3288	22.2656	24.2863	26.7042	30.677	33.9163
plain ALS				0.1000					52.2921			
0.1	TS-ALS	$D = 10$	1.2927	1.0001	0.8641	0.7749	0.7119	15.597	16.2406	15.908	16.1767	17.4988
		$D = 15$	1.0632	0.8798	0.7978	0.7235	0.6728	16.1131	16.0404	16.7699	17.8976	17.3802
		$D = 20$	0.7951	0.6911	0.6223	0.5725	0.5416	16.3257	17.7667	18.1851	18.3393	18.5008
	FCS-ALS	$D = 10$	0.8283	0.7012	0.6326	0.5796	0.5510	18.9016	19.3911	20.3741	22.9006	24.1979
		$D = 15$	0.7505	0.6546	0.5997	0.5523	0.5232	19.7293	21.1838	23.2389	26.2481	28.1806
		$D = 20$	0.5989	0.5291	0.4921	0.4637	0.4424	22.3568	23.8313	26.1499	29.7723	31.3613
plain ALS				0.3162					53.2564			

4.2. Tensor regression network compression

TRNs replace the last flattening and fully-connected layer of convolutional neural networks by tensor regression layer (TRL) [33]. Here, we show the weight tensor of TRL $\mathcal{W} \in \mathbb{R}^{I_1 \times \dots \times I_N \times C}$ (C represents the number of classes) can be compressed by FCS. Denote $\mathcal{X} \in \mathbb{R}^{B \times I_1 \times \dots \times I_N}$ (B represents batch size) as the input activation tensor. Then the output of TRL is

$$\mathbf{Y}(i, j) = \langle \mathbf{X}_{(1)}(i, :)^T, \mathbf{W}_{(N+1)}(j, :)^T \rangle + b. \quad (19)$$

for $i \in [B], j \in [C]$. Hence we can approximate (19) by

$$\hat{\mathbf{Y}}(i, j) = \langle \text{FCS}(\mathbf{X}_{(1)}(i, :)^T), \text{FCS}(\mathbf{W}_{(N+1)}(j, :)^T) \rangle + b, \quad (20)$$

which equals the compact form

$$\hat{\mathbf{Y}} = \text{FCS}(\mathbf{X}_{(1)}^T)^T \text{FCS}(\mathbf{W}_{(N+1)}^T) + \mathbf{b}. \quad (21)$$

The compression ratio (CR) for FCS based TRL is $(\prod_{n=1}^N I_n) / (\sum_{n=1}^N J_n - N + 1) = \tilde{I} / \tilde{J}$.

In this experiment, we compare the performance of CS, TS and FCS based TRL on dataset FMNIST [37] ($C = 10$). The TRL model is composed of two convolutional and maxpooling layers. We assume the regression weight tensor admits low-rank CPD (i.e., CP-TRL [38]) with the target CP rank set as 5. By default, the input activation \mathcal{X} fed to the TRL is of size $B \times 7 \times 7 \times 32$.

We show the network structure in Fig. 4 and comparison results in Table 4. It can be seen that FCS achieves better classification performance than

CS and TS under almost all CRs.

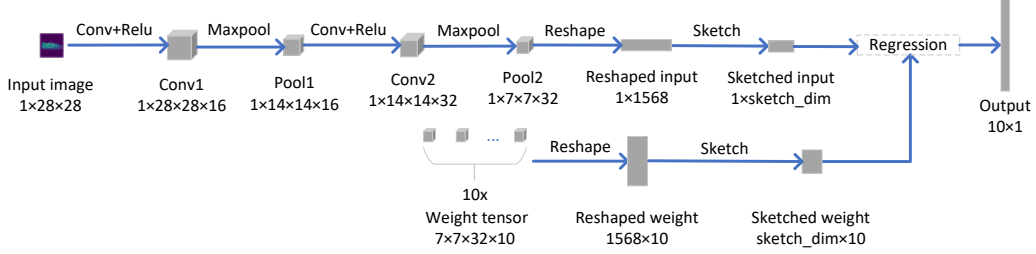


Figure 4: The network structure illustration for the sketching based CP-TRL. The batch size is set to 1 for convenience of display.

Table 4: Classification accuracy by CS, TS and FCS based CP-TRL on dataset FMNIST under various CRs.

CR	20	22.22	25	28.57	33.33	40	50	66.67	100	200
CS	0.7862	0.7529	0.7743	0.7748	0.7451	0.7333	0.7555	0.7322	0.7732	0.7104
TS	0.7461	0.7587	0.7161	0.7665	0.7438	0.6446	0.6871	0.6735	0.7123	0.6999
FCS	0.7829	0.8011	0.7874	0.7815	0.7881	0.7697	0.7706	0.7865	0.7830	0.7696

4.3. Kronecker product and tensor contraction compression

We further compare the performance of FCS against CS and HCS in the Kronecker product compression under the same CRs. We set the independent number of sketches $D = 20$ for all sketching methods.

4.3.1. Kronecker product compression

For two matrices $\mathbf{A} \in \mathbb{R}^{I_1 \times I_2}$, $\mathbf{B} \in \mathbb{R}^{I_3 \times I_4}$, we can compress the Kronecker product $\mathbf{A} \otimes \mathbf{B} \in \mathbb{R}^{I_1 I_3 \times I_2 I_4}$ using FCS by:

$$\begin{aligned} & \text{FCS}(\mathbf{A} \otimes \mathbf{B}; \{\mathbf{h}_n, \mathbf{s}_n\}_{n=1}^4) \\ &= \text{F}^{-1}(\text{F}(\text{CS}(\text{vec}(\mathbf{A}); \{\mathbf{h}_n, \mathbf{s}_n\}_{n=1}^2), \tilde{\mathcal{J}}) * \text{F}(\text{CS}(\text{vec}(\mathbf{B}); \{\mathbf{h}_n, \mathbf{s}_n\}_{n=3}^4), \tilde{\mathcal{J}})), \end{aligned}$$

and the decompressing rule is

$$\widehat{\mathbf{A} \otimes \mathbf{B}}_{I_3(i_1-1)+i_3, I_4(i_2-1)+i_4}$$

$$= \mathbf{s}_1(i_1) \mathbf{s}_2(i_2) \mathbf{s}_3(i_3) \mathbf{s}_4(i_4) \text{FCS}(\mathbf{A} \otimes \mathbf{B})_{\text{mod}(\mathbf{h}_1(i_1)+\mathbf{h}_2(i_2)+\mathbf{h}_3(i_3)+\mathbf{h}_4(i_4)-4, 4J-3)+1},$$

where $i_n \in [I_n]$, J is the Hash length, $\tilde{J} = 4J - 3$. We generate two matrices $\mathbf{A} \in \mathbb{R}^{30 \times 40}$, $\mathbf{B} \in \mathbb{R}^{40 \times 50}$ with each entry randomly drawn from uniform distribution $[-5, 5]$. We compare the compressing time, decompressing time, relative error, and memory cost for Hash functions of CS, HCS and FCS under various CRs. The comparison results are shown in Fig. 5. Clearly, the compressing time of FCS is shorter than CS when CR is small. Although the compressing time of FCS is longer than CS when CR equals 16, we argue it is acceptable, since the relative errors of all compared methods are higher than 1 when CR is 16, which means the accuracy is even worse than the all-zero recovery. Therefore, in practice we should focus on lower compression ratios with relative errors much smaller than 1. Besides, although the compressing speed of HCS is faster, it has larger relative error and much longer decompressing time. Finally, the Hash memory required by FCS is only a ten percent of the Hash memory of CS.

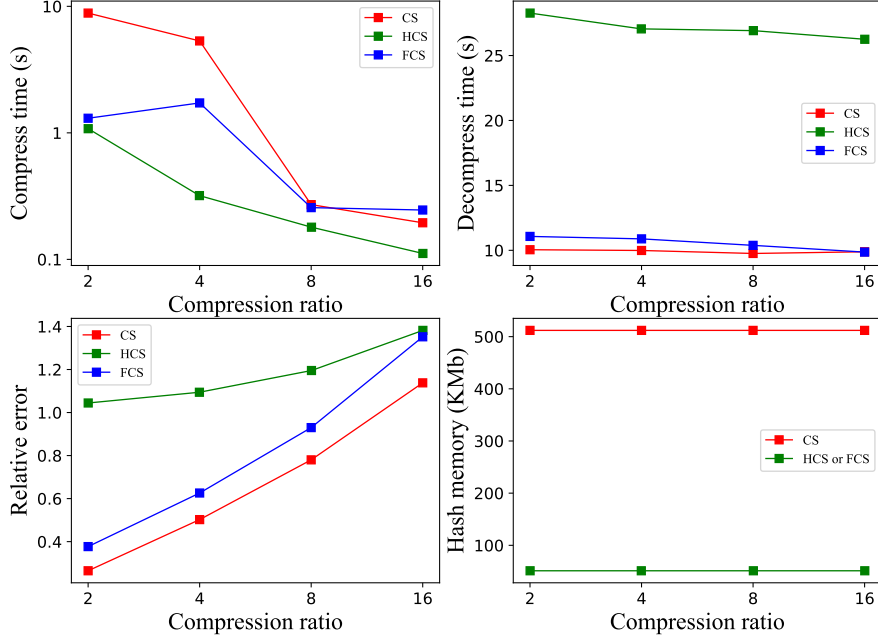


Figure 5: Compressing time, decompressing time, relative error, and memory for Hash functions for CS, HCS and FCS based Kronecker product.

4.3.2. Tensor contraction compression

Given two tensors $\mathcal{A} \in \mathbb{R}^{I_1 \times I_2 \times L}$ and $\mathcal{B} \in \mathbb{R}^{L \times I_3 \times I_4}$ with each entry randomly drawn from $[0, 10]$, the tensor contraction on the third mode of \mathcal{A} and first mode of \mathcal{B} produces a tensor $\mathcal{A} \circledast_{3,1} \mathcal{B} \in \mathbb{R}^{I_1 \times I_2 \times I_3 \times I_4}$. By applying FCS, we approximately compress the contraction by:

$$\begin{aligned} & \text{FCS}(\mathcal{A} \circledast_{3,1} \mathcal{B}; \{\mathbf{h}_n, \mathbf{s}_n\}_{n=1}^4) \\ &= \sum_{l=1}^L \text{F}^{-1}(\text{F}(\text{CS}(\text{vec}(\mathbf{A}(:, :, l)); \{\mathbf{h}_n, \mathbf{s}_n\}_{n=1}^2), \tilde{\mathcal{J}}) * \text{F}(\text{CS}(\text{vec}(\mathbf{B}(l, :, :)); \{\mathbf{h}_n, \mathbf{s}_n\}_{n=3}^4), \tilde{\mathcal{J}})), \end{aligned}$$

And the decompressing rule is

$$\begin{aligned} & \widehat{\mathcal{A} \circledast_{3,1} \mathcal{B}}_{i_1, i_2, i_3, i_4} \\ &= \mathbf{s}_1(i_1) \mathbf{s}_2(i_2) \mathbf{s}_3(i_3) \mathbf{s}_4(i_4) \text{FCS}(\mathcal{A} \circledast_{3,1} \mathcal{B})_{\text{mod}(\mathbf{h}_1(i_1) + \mathbf{h}_2(i_2) + \mathbf{h}_3(i_3) + \mathbf{h}_4(i_4) - 4, 4J - 3) + 1}, \end{aligned}$$

where $i_n \in [I_n]$, J is the Hash length, $\tilde{J} = 4J - 3$. We generate $\mathcal{A} \in \mathbb{R}^{30 \times 40 \times 50}$ and $\mathcal{B} \in \mathbb{R}^{50 \times 40 \times 30}$ with each entry randomly drawn from $[0, 10]$. The comparison results are shown in Fig. 6. Again, when CR is small, FCS has faster compressing speed than CS, faster decompressing speed than HCS and higher accuracy than HCS. And the Hash memory is about 5 percent of CS.

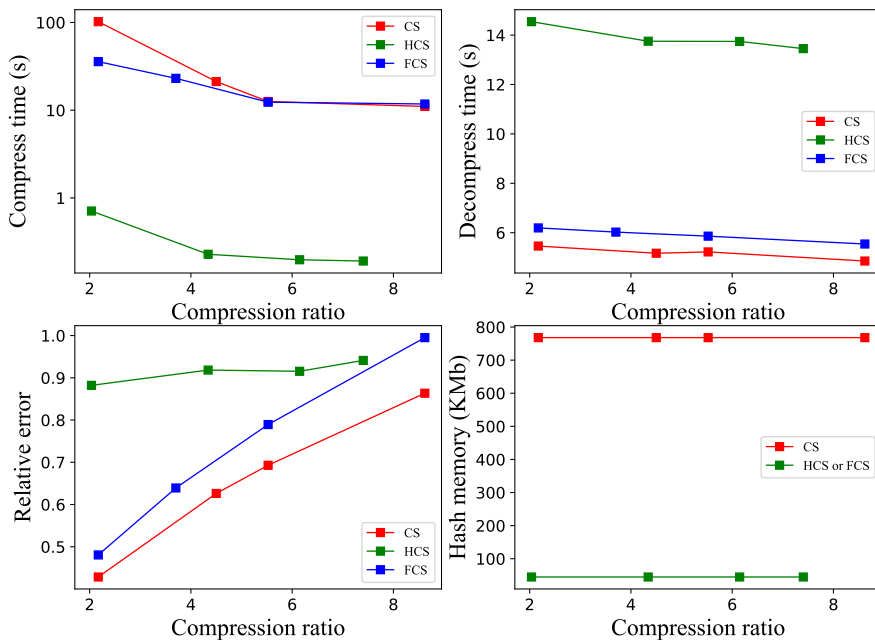


Figure 6: Compressing time, decompressing time, relative error, and memory for Hash functions for CS, HCS and FCS based tensor contraction.

5. Conclusion

A novel sketching method dubbed FCS is presented, which applies multiple shorter Hash functions based CS on the vectorized input tensor. We apply FCS to approximate tensor contraction with the validity guaranteed by theoretical proofs. Numerical experiments on CPD, TRN compression, Kronecker

product and tensor contraction compression confirm that FCS achieves competitive approximation quality and running speed compared with various sketching methods.

References

- [1] R. Guhaniyogi, S. Qamar, D. Dunson, Bayesian tensor regression, *Journal Of Machine Learning Research* 18 (2017) 1–31.
- [2] J. Liu, C. Zhu, Z. Long, H. Huang, Y. Liu, Low-rank tensor ring learning for multi-linear regression, *Pattern Recognition* 113 (2021) 107753.
- [3] J. Liu, P. Musialski, P. Wonka, J. Ye, Tensor completion for estimating missing values in visual data, *IEEE Transactions on Pattern Analysis and Machine Intelligence* 35 (1) (2013) 208–220.
- [4] L. Feng, Y. Liu, L. Chen, X. Zhang, C. Zhu, Robust block tensor principal component analysis, *Signal Processing* 166 (2020) 107271.
- [5] A. Anandkumar, R. Ge, D. Hsu, S. Kakade, M. Telgarsky, Tensor decompositions for learning latent variable models, *Journal Of Machine Learning Research* 15 (2014) 2773–2832.
- [6] A. Anandkumar, R. Ge, M. Janzamin, Guaranteed non-orthogonal tensor decomposition via alternating rank-1 updates, *arXiv preprint arXiv:1402.5180* (2014).
- [7] Y. Wang, H.-Y. Tung, A. J. Smola, A. Anandkumar, Fast and guaranteed tensor decomposition via sketching, *Advances in Neural Information Processing Systems* 28 (2015) 991–999.

- [8] H. Huang, Y. Liu, J. Liu, C. Zhu, Provable tensor ring completion, *Signal Processing* 171 (2020) 107486.
- [9] M. J. Reynolds, A. Doostan, G. Beylkin, Randomized alternating least squares for canonical tensor decompositions: Application to a pde with random data, *SIAM Journal on Scientific Computing* 38 (5) (2016) 2634–2664.
- [10] C. Battaglino, G. Ballard, T. G. Kolda, A practical randomized cp tensor decomposition, *SIAM Journal on Matrix Analysis and Applications* 39 (2) (2018) 876–901.
- [11] L. Yuan, C. Li, J. Cao, Q. Zhao, Randomized tensor ring decomposition and its application to large-scale data reconstruction, in: *ICASSP 2019 - 2019 IEEE International Conference on Acoustics, Speech and Signal Processing (ICASSP)*, Vol. 2019-, IEEE, 2019, pp. 2127–2131.
- [12] R. Minster, A. K. Saibaba, M. E. Kilmer, Randomized algorithms for low-rank tensor decompositions in the tucker format, *SIAM Journal on Mathematics of Data Science* 2 (1) (2020) 189–215.
- [13] B. Rakhshan, G. Rabusseau, Tensorized random projections, in: *International Conference on Artificial Intelligence and Statistics*, PMLR, 2020, pp. 3306–3316.
- [14] T. Sarlos, Improved approximation algorithms for large matrices via random projections, in: *2006 47th Annual IEEE Symposium on Foundations of Computer Science (FOCS'06)*, IEEE, 2006, pp. 143–152.

- [15] K. Clarkson, D. Woodruff, Low-rank approximation and regression in input sparsity time, *Journal of the ACM (JACM)* 63 (6) (2017) 1–45.
- [16] K. L. Clarkson, D. P. Woodruff, Numerical linear algebra in the streaming model, in: *Proceedings of the forty-first annual ACM symposium on Theory of computing*, 2009, pp. 205–214.
- [17] D. P. Woodruff, Sketching as a tool for numerical linear algebra 10 (1-2) (2014).
- [18] A. Chowdhury, J. Yang, P. Drineas, An iterative, sketching-based framework for ridge regression, in: *International Conference on Machine Learning*, PMLR, 2018, pp. 989–998.
- [19] M. Charikar, K. Chen, M. Farach-Colton, Finding frequent items in data streams, *Automata, Languages And Programming* 2380 (2002) 693–703.
- [20] R. Pagh, Compressed matrix multiplication, *ACM Transactions on Computation Theory (TOCT)* 5 (3) (2013) 1–17.
- [21] N. Pham, R. Pagh, Fast and scalable polynomial kernels via explicit feature maps, in: *Proceedings of the 19th ACM SIGKDD international conference on knowledge discovery and data mining*, Vol. 128815 of *KDD '13*, ACM, 2013, pp. 239–247.
- [22] B. Yang, A. Zamzam, N. D. Sidiropoulos, Parasketch: Parallel tensor factorization via sketching, in: *Proceedings of the 2018 SIAM International Conference on Data Mining*, SIAM, 2018, pp. 396–404.

- [23] O. A. Malik, S. Becker, Low-rank tucker decomposition of large tensors using tensorsketch, *Advances in neural information processing systems* 31 (2018) 10096–10106.
- [24] Y. Sun, Y. Guo, C. Luo, J. Tropp, M. Udell, Low-rank tucker approximation of a tensor from streaming data, *SIAM Journal on Mathematics of Data Science* 2 (4) (2020) 1123–1150.
- [25] H. Diao, Z. Song, W. Sun, D. Woodruff, Sketching for kronecker product regression and p-splines, in: *International Conference on Artificial Intelligence and Statistics*, PMLR, 2018, pp. 1299–1308.
- [26] H. Diao, R. Jayaram, Z. Song, W. Sun, D. Woodruff, Optimal sketching for kronecker product regression and low rank approximation, in: *Advances in Neural Information Processing Systems*, 2019, pp. 4737–4748.
- [27] S. P. Kasiviswanathan, N. Narodytska, H. Jin, Network approximation using tensor sketching., in: *IJCAI*, 2018, pp. 2319–2325.
- [28] I. Han, H. Avron, J. Shin, Polynomial tensor sketch for element-wise function of low-rank matrix, in: *International Conference on Machine Learning*, PMLR, 2020, pp. 3984–3993.
- [29] Y. Shi, Efficient tensor operations via compression and parallel computation, Ph.D. thesis, UC Irvine (2019).
- [30] J. Carroll, J.-J. Chang, Analysis of individual differences in multidimensional scaling via an n-way generalization of “eckart-young” decomposition, *Psychometrika* 35 (3) (1970) 283–319.

- [31] R. A. Harshman, et al., Foundations of the parafac procedure: Models and conditions for an “explanatory” multimodal factor analysis (1970).
- [32] T. G. Kolda, B. W. Bader, Tensor decompositions and applications, *SIAM Review* 51 (3) (2009) 455–500.
- [33] J. Kossaifi, Z. C. Lipton, A. Kolbeinsson, A. Khanna, T. Furlanello, A. Anandkumar, Tensor regression networks, *Journal of Machine Learning Research* 21 (2020) 1–21.
- [34] A. Anandkumar, R. Ge, M. Janzamin, Analyzing tensor power method dynamics in overcomplete regime, *Journal Of Machine Learning Research* 18 (2017) 1–40.
- [35] F. Yasuma, T. Mitsunaga, D. Iso, S. K. Nayar, Generalized assorted pixel camera: postcapture control of resolution, dynamic range, and spectrum, *IEEE transactions on image processing* 19 (9) (2010) 2241–2253.
- [36] S. Wanner, S. Meister, B. Goldluecke, Datasets and benchmarks for densely sampled 4d light fields., in: *VMV*, Vol. 13, Citeseer, 2013, pp. 225–226.
- [37] H. Xiao, K. Rasul, R. Vollgraf, Fashion-mnist: a novel image dataset for benchmarking machine learning algorithms, *arXiv preprint arXiv:1708.07747* (2017).
- [38] X. Cao, G. Rabusseau, Tensor regression networks with various low-rank tensor approximations, *arXiv preprint arXiv:1712.09520* (2017).